

Global impacts of transportation infrastructure on forest degradation and loss

Received: 18 March 2025

Accepted: 22 January 2026

Published online: 04 February 2026

 Check for updates

Decheng Zhou¹, Jingfeng Xiao²✉, Shuguang Liu¹, Lin Huang³,
Liangxia Zhang¹, Jiangwen Fan³ & Shuqing Zhao¹✉

Transportation networks threaten global forests, but prior assessments have been regional or limited to single metrics (e.g., forest cover). Here, we present a global analysis of multidimensional road effects on forests, using high-resolution remote sensing data and a Grid-wise Environmental Matching for Background Reference (GEM-BR) strategy. We detect 18.6% lower forest cover, 2.7 m shorter canopy height, 52.2 gC m⁻² yr⁻¹ reduced net primary productivity, and 23.0 patches per km² higher fragmentation within 1 km of roads compared to reference areas. Impacts extend up to 5 km with a clear distance decay effect, totaling 4.26 million km² of forest loss—equivalent to 10.7% of the 2020 global forest extent. The Global South (tropics accounting for 54.8%) faces severe, worsening degradation (2000–2020), while the Global North shows milder impacts, with partial recovery. Critically, 89% of grid cells exhibit conflicting long-term trends across metrics, highlighting the inadequacy of cover-only assessments. We further find that road-linked degradation is tightly coupled with local human activity, and that global protected areas have insufficient capacity to curb ongoing degradation. Differences in impacts among regions suggest that road-linked forest degradation is tied to governance choices—urging integrated transport-forest planning to balance development and conservation.

Transportation infrastructure is a cornerstone of economic vitality, facilitating the movement of people and goods while enabling access to natural resources and arable land¹. Nevertheless, roads and railways often degrade ecosystems—particularly in pristine, conservation-critical areas—by opening wilderness to logging, colonization, hunting, and mining, which drive habitat loss and species decline^{2–9}. With rising demand for resources and development initiatives, transportation networks are expanding unprecedentedly: they are projected to grow by over 60% globally between 2010 and 2050, with most expansion in developing nations¹⁰. This trend has intensified concerns among scientists and planners about infrastructure-driven threats to natural ecosystems.

Forests are central to addressing anthropogenic disturbances, as they harbor 80% of terrestrial biodiversity and act as the largest terrestrial carbon sink^{6,11,12}. Whereas transportation expansion poses a severe risk, especially in the tropics^{5,13–15}: -17% of tropical moist forests have been lost since 1990¹⁶, a trend likely to persist given that road construction is promoted as a strategy for employment and regional development⁷. Meeting the Paris Agreement’s temperature targets—via the COP28 pledge to “halt and reverse deforestation by 2030”¹⁷—depends on comprehensive assessments of transportation’s impacts to guide effective forest conservation and restoration. While prior studies have investigated forest degradation and loss across scales^{9,13,14,16,18–24}, few have isolated transportation infrastructure’s

¹Center for Eco-Environment Restoration of Hainan Province/Hainan Baoting Tropical Forest Ecosystem Observation and Research Station, School of Ecology, Hainan University, Haikou, China. ²Earth Systems Research Center, Institute for the Study of Earth, Oceans, and Space, University of New Hampshire, Durham, NH, USA. ³Key Laboratory of Land Surface Pattern and Simulation, Institute of Geographic Sciences and Natural Resources Research, Chinese Academy of Sciences, Beijing, China. ✉e-mail: j.xiao@unh.edu; shuqing.zhao@hainanu.edu.cn

specific effects at the global level. Existing work focuses largely on tropical road-driven forest loss^{2,4,5,7,25}, neglecting impacts on landscape fragmentation, forest height, and associated ecosystem functions^{26,27}. Moreover, temperate and boreal forests—extensive in coverage²⁸ and subject to high human activity²⁹—remain understudied. This leaves a critical gap: how transportation infrastructure impacts forests multidimensionally, and how these effects vary spatially and temporally.

Here, we present a global, multifaceted evaluation of road-linked forest degradation, integrating high-resolution satellite data with transportation infrastructure records. We quantify forest structure and function at a 1 km spatial resolution using four robust metrics: three structural indicators—forest cover (percentage of grid cell occupied by forest), patch density (PD; number of forest patches per km²), and mean height (average canopy height)—and one functional indicator, mean net primary productivity (NPP; a proxy for carbon sequestration). These metrics collectively capture forest integrity, with established links to biodiversity conservation and climate mitigation potential^{19,30–32}.

To systematically quantify road impacts, we develop a three-step analytical framework (Supplementary Fig. 1; Methods). First, we focus on “forested grid cells” (1-km cells with >0% forest cover in 2000 or 2020; Supplementary Fig. 2a, b) to target areas with existing or historical forest. Second, we stratify these grid cells into three proximity zones—road zones (0–1 km, strong impact), road-reference interface (RRI; 1–5 km, partial impact), and “other” zones (>5 km, minimal impact, potential references)—aligned with prior work on distance-dependent road effects^{4,6,25,33}. These zones are delineated using two global road datasets: OpenStreetMap (OSM)³⁴, as the primary source, supplemented with the Global Roads Inventory Project version 4 (GRIP4)¹⁰. This integration of these two datasets enhances road coverage by capturing roads exclusively documented in GRIP4, resulting in an 11% increase in the estimated road zone area (see Methods for details). Third, we calculate road impacts (δI) as absolute ($I_{\text{road}} - I_{\text{ref}}$) and normalized relative [$(I_{\text{road}} - I_{\text{ref}}) / (|I_{\text{road}}| + |I_{\text{ref}}|) \times 100\%$] disparities, where I_{road} denotes metric values in road/RRI zones, and I_{ref} denotes background reference values. To derive I_{ref} , we develop a “Grid-wise Environmental Matching for Background Reference (GEM-BR)” strategy, which selects reference cells by environmental similarity to minimize confounding inherent differences—such as lower rates of road building and forest degradation in sloping terrain. Negative values for δCover (where δ denotes the difference in road/RRI zones relative to reference areas; hereafter for all δ metrics), δHeight , and δNPP , and positive values for δPD indicate forest degradation; inverse patterns indicate improvement. We evaluate these road impacts across two key dimensions—2020 current state and 2000–2020 long-term changes—and also assess distance decay effects up to 5 km to quantify total road impact areas. We further contextualize these road impacts by examining their relationships with human activity—using the Human Footprint Index (HFI)²⁹ and nighttime lights (NTL)³⁵—and protected area coverage.

We find widespread multidimensional forest degradation in road-adjacent areas globally, with far more severe and worsening impacts in the Global South than the Global North. These effects are tightly coupled with human activity intensity yet poorly mitigated by protected areas, filling a critical gap in understanding road-forest-human interactions at global scales. This integrated analysis advances quantification of road impacts across nested spatial levels, with findings informing evidence-based transport-forest planning—key to balancing infrastructure development and conservation goals.

Results

Impacts of transportation infrastructure on current forest state
Compared to reference zones, road-adjacent areas show widespread forest degradation globally (Fig. 1), characterized by reduced forest cover, height, and NPP, alongside increased PD. In 2020, this

degradation is observed across 53–69% of all forested grid cells. The global average road-reference disparities (δ) are: $\delta\text{Cover} = -18.6\%$ (relative change: -22.4%), $\delta\text{Height} = -2.7\text{ m}$ (-10.5%), $\delta\text{NPP} = -52.2\text{ gC m}^{-2}\text{ yr}^{-1}$ (-2.7%), and $\delta\text{PD} = +23.0\text{ patches km}^{-2}$ ($+9.3\%$) (Fig. 2).

Road impacts exhibit marked spatial variability, with stronger effects concentrated in mid-to-low latitudes (Fig. 1). By climate zone, tropical regions show the largest absolute declines in δCover (-23.2%) and δHeight (-4.4 m), arid zones the steepest δPD increase ($+35.2\text{ patches km}^{-2}$), and polar zones the greatest absolute δNPP reduction ($-147\text{ gC m}^{-2}\text{ yr}^{-1}$) (Fig. 2a–d). When normalized to background reference values (Supplementary Fig. 3), relative changes (Fig. 2e–h) reveal that tropical zones are most vulnerable to height loss, while arid zones face the severest cover loss and polar zones the largest NPP decline. Notably, arid, cold, and polar zones show statistically significant relative δPD decreases—contrasting with relative increases in tropical and temperate zones.

At continental and national scales, degradation is most severe in South America, Asia, and Africa, whereas Europe exhibits positive δNPP ($+26.3\text{ gC m}^{-2}\text{ yr}^{-1}$). Country-level patterns (Supplementary Fig. 4) highlight acute degradation in South Asian (e.g., Cambodia, Thailand), African (e.g., Burundi, Rwanda), and South American (e.g., Colombia, Ecuador) nations, versus improvement in northwestern European countries (e.g., Norway, Sweden). This forms a clear global divide (Fig. 2e–h): impacts are far more severe in the Global South than the Global North, with larger relative declines in δCover (-25.7% vs. -15.9%) and δHeight (-13.9% vs. -3.5%), opposing δPD trends ($+15.6\%$ vs. -2.9%), and contrasting δNPP (-4.3% vs. $+0.4\%$).

Road impacts extend into the 1–5 km RRI zones, with a strong distance decay effect: mean impacts in RRI zones are $\sim 50\%$ of those in road zones (Supplementary Fig. 5), though this intensity is far more pronounced in tropical zones, South America, Africa, and the Global South. Accounting for total forest extent in road/RRI zones (Supplementary Fig. 2), we estimate global forest area loss in these zones at 4.26 million km² relative to background references (equivalent to 10.7% of 2020 global forest extent or 2.17 times Mexico’s area) (Supplementary Fig. 6a, b), with 71% occurring in road zones alone (Supplementary Fig. 6c). Tropical regions contribute 54.8% of this loss, and Asia, Africa, and South America collectively account for 81.9% (Supplementary Fig. 6b). The top five contributing nations—Brazil (13.6%), Russia (11.4%), China (7.7%), Republic of the Congo (4.2%), and Australia (3.4%)—reflect their large forest extents and high road impact intensities (Supplementary Fig. 6a). The Global South is responsible for 78.2% of total road/RRI-linked forest loss (Supplementary Fig. 6b).

Long-term changes in road-linked forest degradation and loss

From 2000 to 2020, global road-linked forest impacts (temporal change denoted as $\Delta\delta I$, i.e., shifts in road-vs-reference disparities) show mixed trends across the four metrics (Fig. 3). On average, road zones exhibit: $\Delta\delta\text{Cover} = -2.5\%$ (relative change: -5.1%), $\Delta\delta\text{PD} = -1.7\text{ patches km}^{-2}$ ($+1.8\%$), $\Delta\delta\text{Height} = -0.2\text{ m}$ (-1.1%), and $\Delta\delta\text{NPP} = -4.8\text{ gC m}^{-2}\text{ yr}^{-1}$ (-0.5%) (Fig. 4).

These long-term changes diverge sharply between the Global South and Global North. The Global South experiences worsening degradation in road zones—particularly in tropical regions (e.g., $\Delta\delta\text{Cover}$: -10.9% relative change; $\Delta\delta\text{Height}$: -5.7% relative change) and across South America and Africa. South America shows relative declines in $\Delta\delta\text{Cover}$ and $\Delta\delta\text{Height}$ of -11.8% and -4.3% , respectively, while Africa records declines of -9.4% and -7.1% (Fig. 4). In contrast, the Global North exhibits smaller overall shifts and even a mean increase in forest height. Europe stands out with consistent improvement over 20 years: relative gains of 4.6% in cover, 4.1% in height, and 2.4% in NPP, plus a 9.4% reduction in PD.

The worsening degradation observed in road zones extends to RRI zones, especially in South America and Africa, where mean

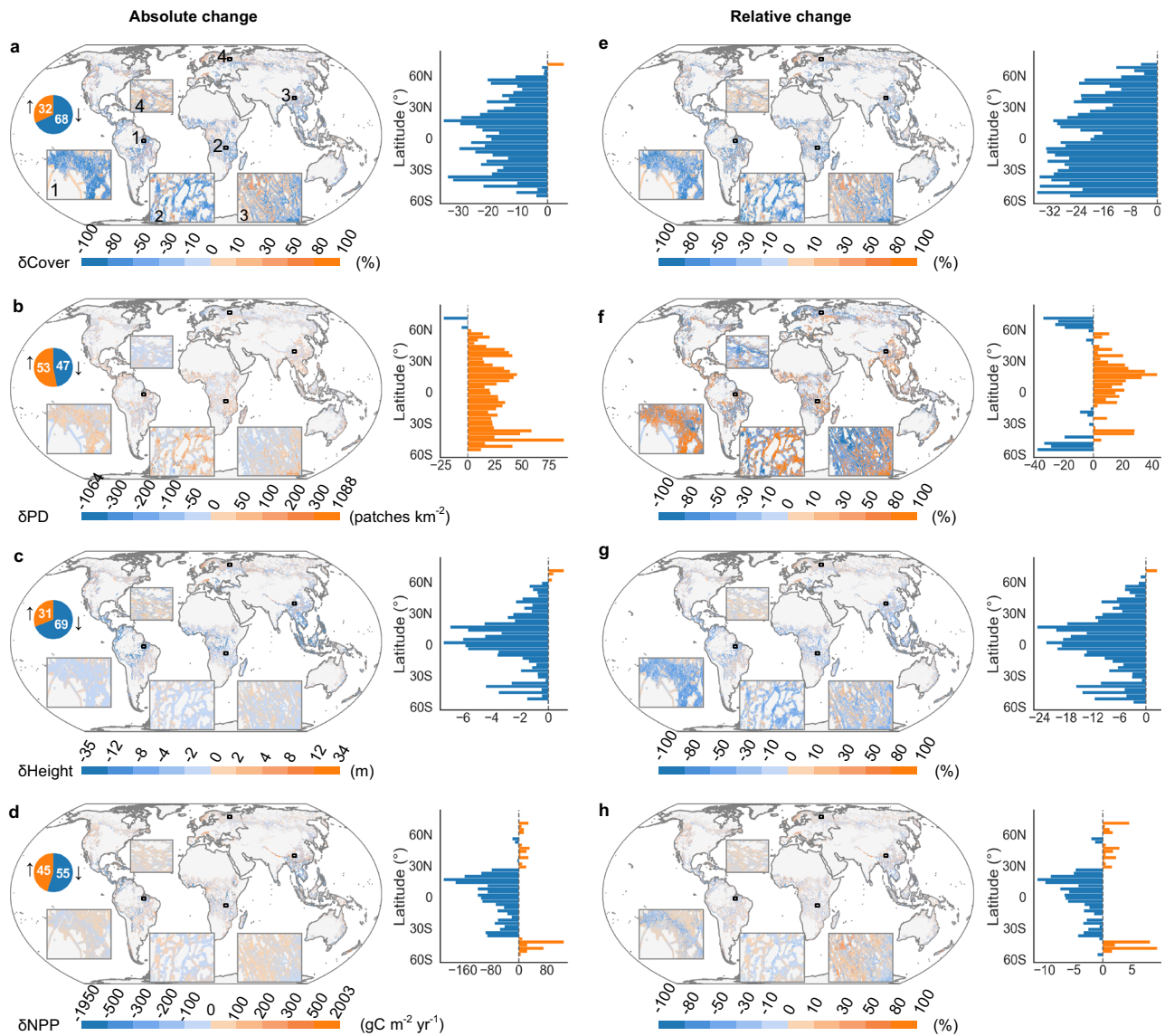


Fig. 1 | Effects of transportation infrastructure on current forest structure and function in road areas (1-km buffer zones) at 1 km resolution (2020). **a–d** Absolute changes and **e–h** normalized relative changes in forest metrics. δCover , δPD , δHeight , and δNPP denote differences in forest cover, patch density, height, and net primary productivity (NPP) between road areas and background references, respectively. Inset pie charts show the frequency of grid cells with

positive (\uparrow) or negative (\downarrow) differences. Insets 1–4 (numbered in **a**) are zoomed-in examples illustrating road impacts: 1, South America; 2, Africa; 3, Asia; 4, Europe. Bar charts depict latitudinal variations across 3° latitude bins. Continental boundaries were obtained from Natural Earth (<https://www.naturalearthdata.com/>). Source data are provided as a Source Data file.

absolute $\Delta\delta\text{I}$ values in 1–2 km RRI zones are comparable to those in road zones (Supplementary Fig. 7). North America shows a distinct pattern: negligible $\Delta\delta\text{NPP}$ changes, similar $\Delta\delta\text{PD}$ and $\Delta\delta\text{Cover}$ shifts, and even larger $\Delta\delta\text{Height}$ changes as compared to road zones (Supplementary Fig. 7e–h). Meanwhile, Asia, Europe, and Oceania exhibit minimal fluctuations in RRI zones overall. Accounting for total forest extent in road/RRI zones, the Global South contributes 90.2% of global increased forest loss between 2000 and 2020 (Supplementary Fig. 6). The top contributors are Brazil (18.2% at the national scale), the tropical zone (76.5% at the climatic scale), and South America (48.4% at the continental scale).

Notably, minimal net $\Delta\delta\text{I}$ values do not indicate static road impacts. Instead, we observe large concurrent forest gains and losses (Supplementary Fig. 8)—most pronounced in the Global North. Here, the area of forest gain (325.7 thousand km^2) is close to that of loss (383.7 thousand km^2). This suggests that road-linked degradation—

from construction or operation—may be partially offset by regional forest regrowth or restoration, explaining the Global North’s small net changes.

Road impact linked to human pressure

Across global forested lands, we find a strong quantitative association between road-linked forest changes and the HFI, with higher values indicating greater pressure (Fig. 5a–d). Specifically, the magnitude of road-vs-reference disparities ($|\delta\text{I}|$) for all four metrics increases significantly with rising HFI, showing robust positive linear correlations for both absolute and relative changes in forest degradation ($R^2 = 0.82\text{--}0.98$, $p < 0.001$, $N = 100$). This trend is most pronounced for relative changes in δPD and δCover . Notably, for δCover , δHeight , and δNPP , the rate of increase in $|\delta\text{I}|$ is substantially steeper when $\text{HFI} < 0.4$. This suggests road-linked degradation may intensify more rapidly in the early stages of increasing human pressure—potentially reflecting a

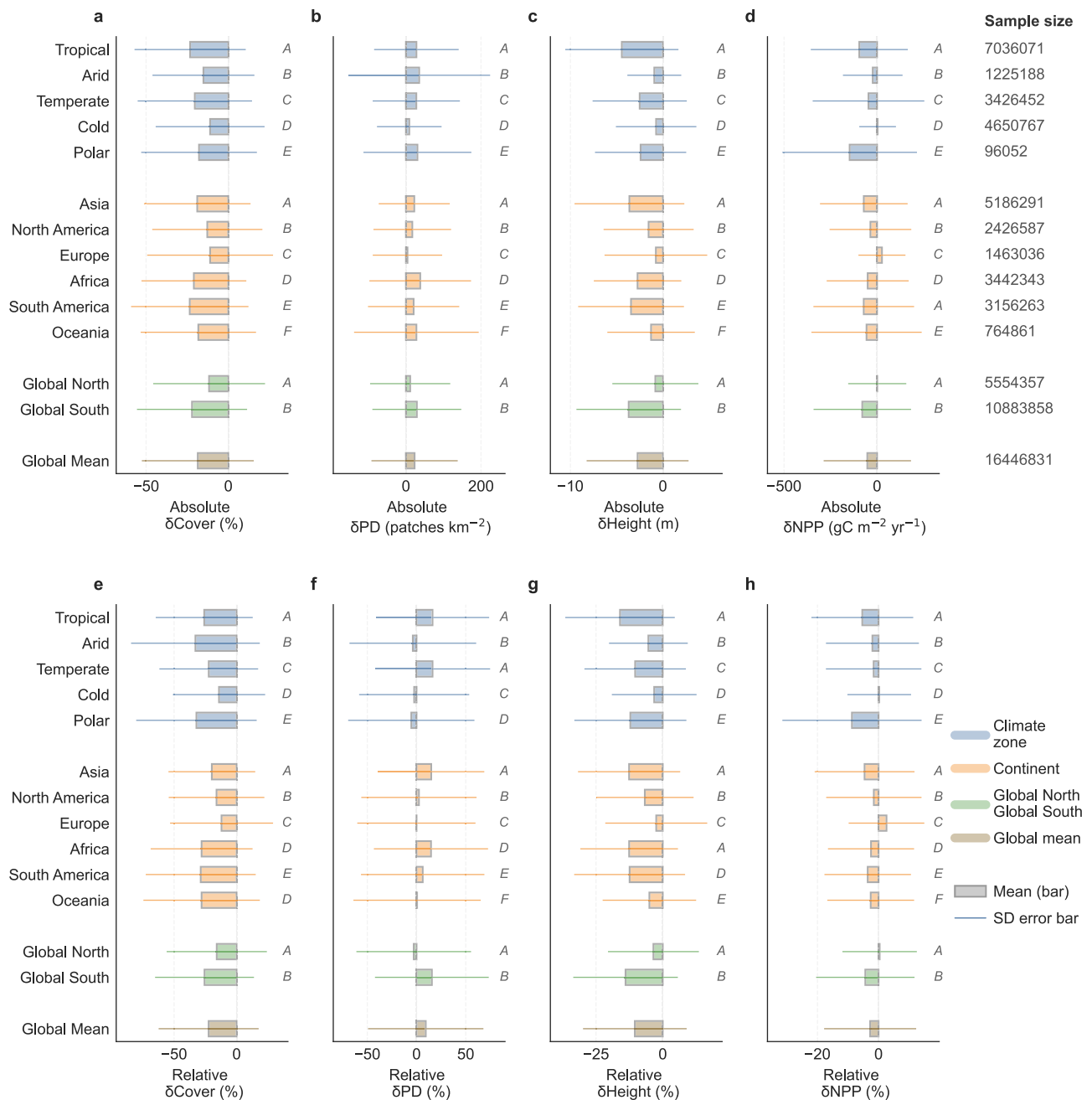


Fig. 2 | Spatial variations in road impacts on current forest structure and function across climate zones, continents, and Global North versus South. **a–d** Absolute changes and **e–h** normalized relative changes in forest metrics. Data are presented as mean values \pm standard deviation (SD). Mean estimates for all groups differ significantly from zero (two-sided *t*-test, $P < 0.05$). Uppercase italic

gray letters indicate significant differences between categories (one-way ANOVA followed by Tukey's HSD test; distinct letters denote significant differences at $P < 0.05$). δ denotes differences between road areas and background references. Source data are provided as a Source Data file.

threshold effect where initial anthropogenic disturbance amplifies the vulnerability of road-adjacent forests.

This association is further supported by long-term temporal changes: 2000–2020 shifts in road impacts ($\Delta\delta I$) for all metrics are closely tied to concurrent HFI changes ($R^2 = 0.57\text{--}0.93$, $p < 0.001$, $N = 100$) (Fig. 5e–h). A clear directional pattern emerges: decreased HFI is associated with increased forest cover and height, along with reduced PD in road zones; increased HFI drives the opposite changes. However, when HFI changes exceed ± 0.3 (relative to baseline), $\Delta\delta I$ values fluctuate sharply. This variability likely reflects complex human activity interactions in highly disturbed regions, where

extensive deforestation (from infrastructure or agriculture) and targeted afforestation/restoration coexist—driving opposing net forest dynamics.

To cross-validate these patterns, we analyze correlations between road-linked forest changes and NTL, another proxy for human activity intensity. The results closely mirror those with HFI: NTL intensity shows statistically strong positive correlations with the magnitude of δI values (i.e., $|\delta I|$) for road-linked degradation (Supplementary Fig. 9), especially at the lower NTL bins. Together, these findings confirm a fundamental relationship: the severity of road-adjacent forest degradation is tightly coupled to local human activity intensity.

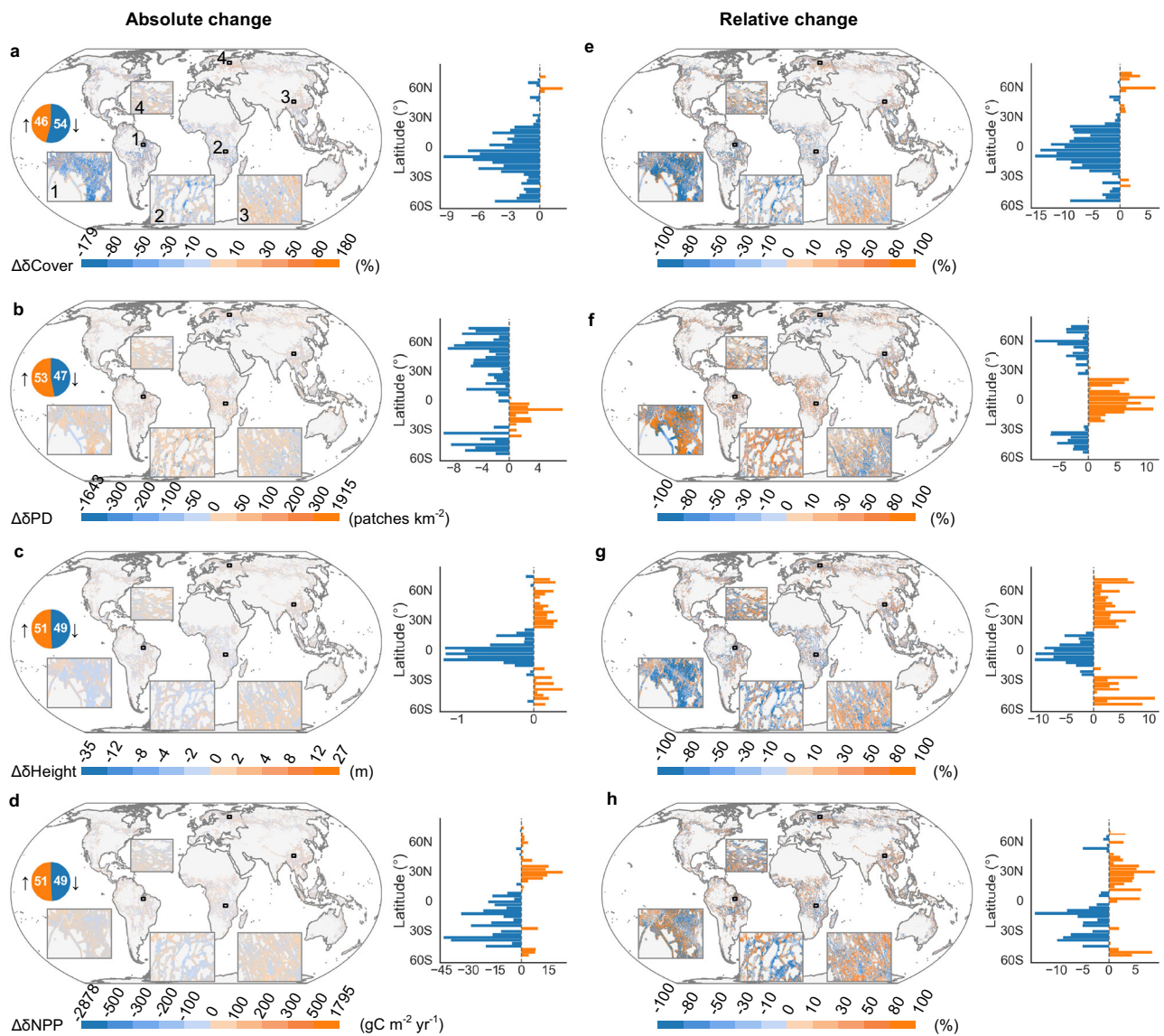


Fig. 3 | Temporal changes in road impacts on forest structure and function in road areas (1 km buffer zones) from 2000 to 2020. a–d Absolute changes and **e–h** normalized relative changes in forest metrics. δ denotes differences between road areas and background references, and Δ indicates temporal changes between 2000 and 2020. Inset pie charts show the frequency of grid cells with positive (\uparrow) or

negative (\downarrow) temporal changes. Insets 1–4 are zoomed-in examples illustrating road impacts: 1, South America; 2, Africa; 3, Asia; 4, Europe. Bar charts depict latitudinal variations across 3° latitude bins. Continental boundaries were obtained from Natural Earth (<https://www.naturalearthdata.com/>). Source data are provided as a Source Data file.

Contrasting road impacts between protected and non-protected areas

For the current forest state, our analysis indicates that global protected areas (PAs) effectively mitigate road-linked degradation. This is evidenced by statistically smaller road impact magnitudes for all metrics in PAs versus non-protected areas (non-PAs)—a pattern consistent globally and across most subregions, with the polar zone as the only exception (Fig. 6). The global contrast is striking: mean relative changes in road-impacted metrics are far milder in PAs, with δ Cover = -16.1% (vs. -20.8% in non-PAs), δ Height = -7.7% (vs. -10.2%), and δ NPP = -1.7% (vs. -2.1%). Notably, PAs even show a slight negative δ PD (marginal reduction in fragmentation relative to references), in sharp contrast to the positive δ PD (increased fragmentation) observed in non-PAs. This protective effect, however, varies sharply by region: among climate zones, temperate zones exhibit the largest reduction in

road-linked degradation in PAs relative to non-PAs, while at the continental scale, Oceania has the strongest protective effect—with PA road impacts far less severe than in adjacent non-protected lands.

Despite these benefits, road-linked degradation remains severe in global PAs—particularly in tropical regions, where mean absolute δ Cover and δ Height reach -16.2% and -3.2 m, respectively. Similarly, South American PAs face notable road pressure (δ Cover = -15.1% , δ Height = -2.6 m). More concerning, 2000–2020 changes show road impacts intensify marginally faster in PAs than in non-PAs—a pattern most evident in Africa, North America, and arid zones (Supplementary Fig. 10). This implies that since the turn of the century, PAs worldwide have largely struggled to curb worsening road-linked degradation. For these ecologically critical areas, this escalating vulnerability highlights a growing disconnect between protection status and the effective mitigation of road-related anthropogenic disturbance.

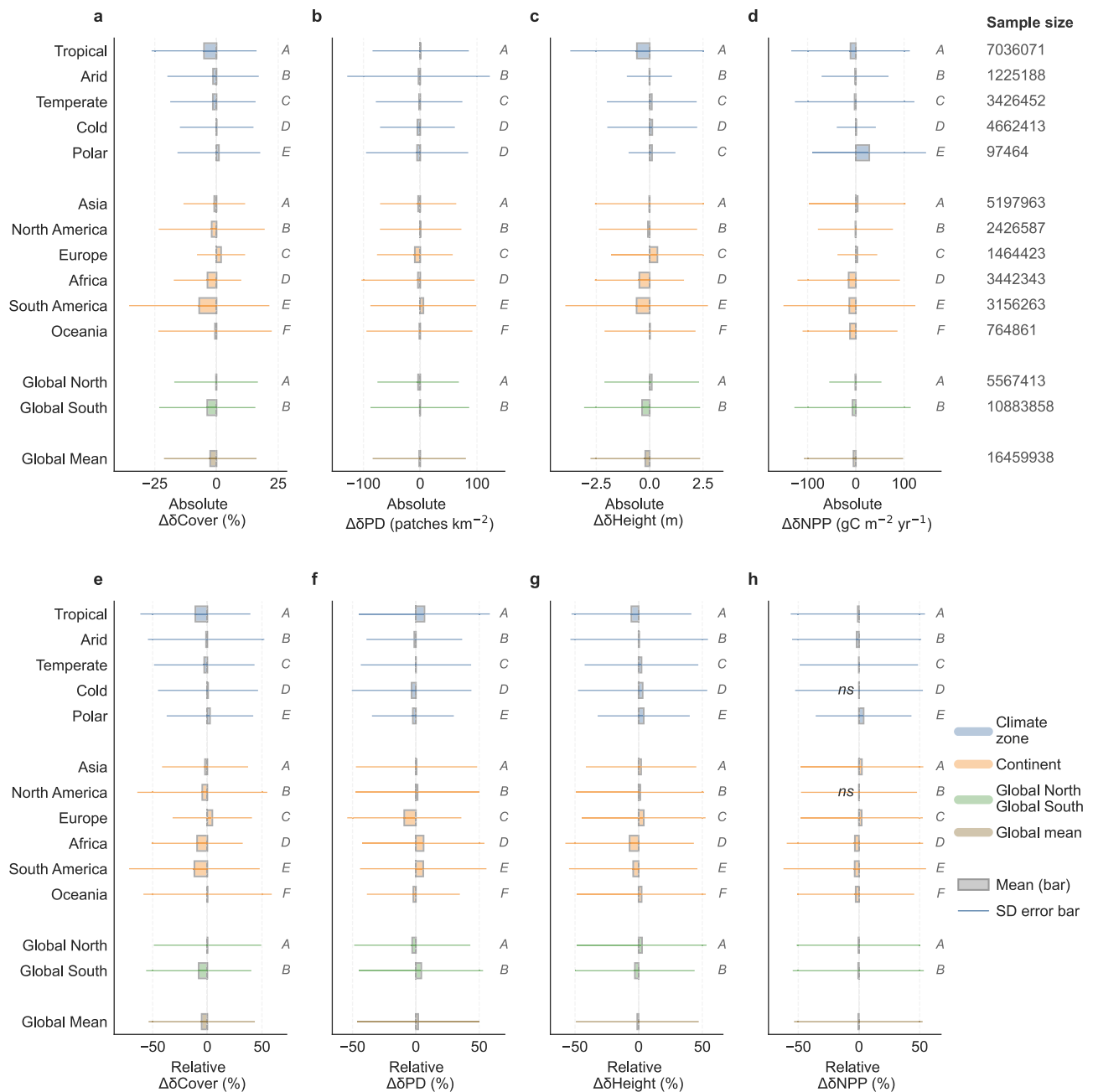


Fig. 4 | Spatial variations in temporal changes of road impacts on forest structure and function across climate zones, continents, and Global North versus South. a–d Absolute changes and **e–h** normalized relative changes in forest metrics. Data are presented as mean values \pm standard deviation (SD). Mean estimates for all groups differ significantly from zero (two-sided *t*-test, $P < 0.05$), except

two marked 'ns'. Uppercase italic gray letters indicate significant differences between categories (one-way ANOVA followed by Tukey's HSD test; distinct letters denote significant differences at $P < 0.05$). δ denotes differences between road areas and background references, and Δ indicates temporal changes between 2000 and 2020. Source data are provided as a Source Data file.

Discussion

Beyond forest cover loss: multidimensional degradation and ecological consequences

Road-linked forest degradation transcends visible cover loss, encompassing coordinated declines in structure (cover and height), connectivity (PD), and function (NPP). This undermines the reliability of area-only conservation metrics. The multidimensional decline poses acute risks to biodiversity and climate mitigation: elevated patch density (i.e., PD)—a metric reflecting more patches per unit area—amplifies edge effects (e.g., microclimate warming, invasive species colonization)¹⁴, which disproportionately harm specialist species

dependent on interior forest conditions and raise their local extinction risk³⁶. Notably, PD itself does not equate to patch isolation (i.e., the spatial distance between patches or their functional connectivity). An increase in PD may arise from large patches fragmenting into small but spatially clustered patches (low isolation) or into widely separated patches (high isolation)³⁷—with distinct ecological consequences, and isolation, when coincident with high PD, exacerbates biodiversity loss by limiting species dispersal and recolonization³⁸. While debates persist in the literature about the independent effect of fragmentation per se (after accounting for habitat loss or isolation)³⁹, evidence suggests that fragmentation—when combined with its associated consequences

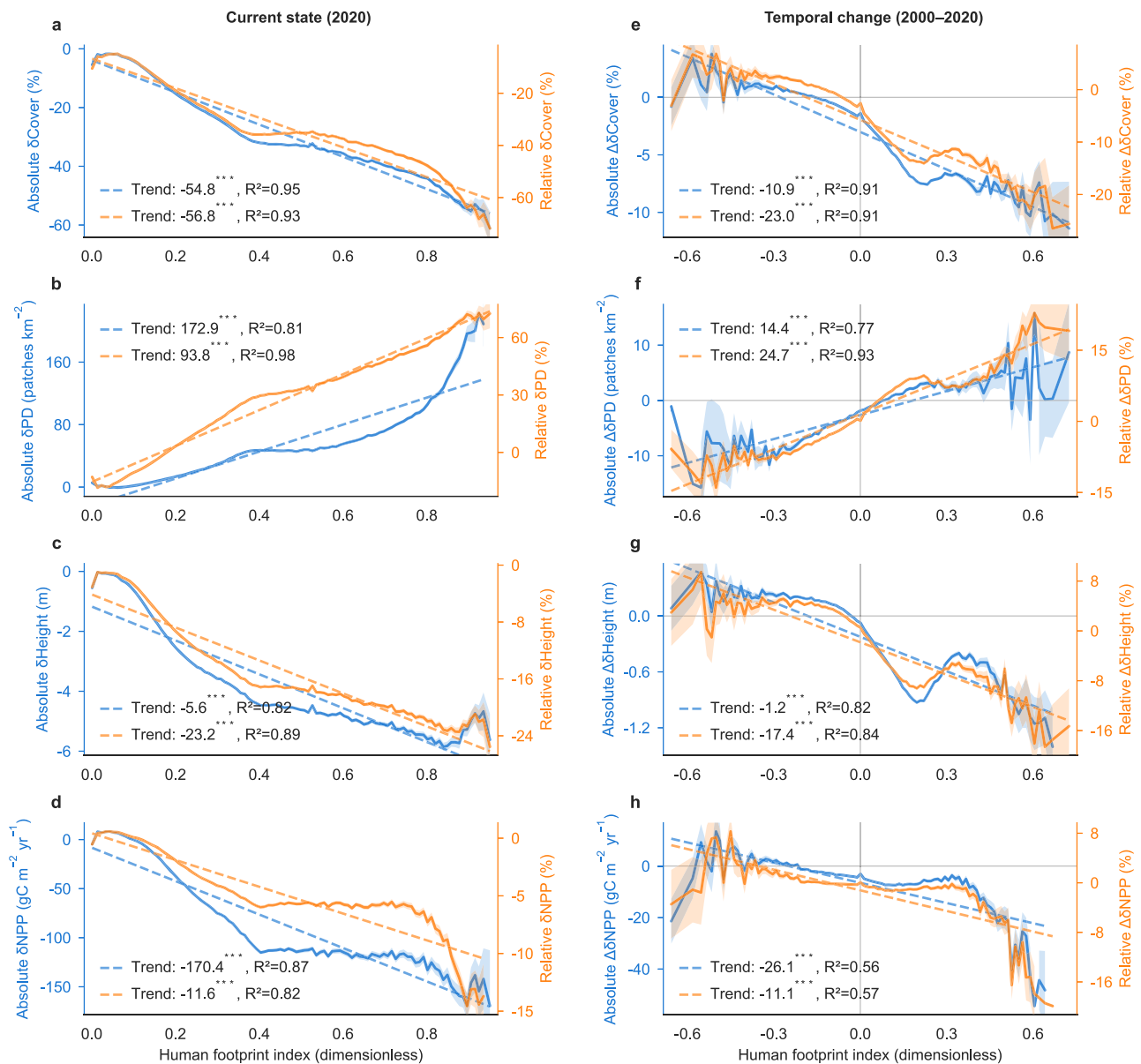


Fig. 5 | Relationship between road impacts and the Human Footprint Index (HFI) across global road zones. a–d Road impacts on the current forest state. **e–h** Temporal changes (2000–2020). HFI was binned into 100 levels by percentiles. Blue and orange curves represent the mean values of absolute and normalized relative changes in forest metrics, respectively. Shaded regions indicate the 95% confidence intervals (CI) around the mean. Dashed lines denote linear

change trends, with annotated values representing trend slopes (Trend) and coefficient of determination (R^2). All trend slopes are statistically significant (two-sided simple linear regression; $P < 0.001$) (**). δ denotes differences between road areas and background references, and Δ indicates temporal changes between 2000 and 2020. Source data are provided as a Source Data file.

(isolation and edge effects)—heightens the likelihood of local population extinction. Global meta-analyses support this: when fragmentation involves both high PD and increased isolation, biodiversity declines by 13–75% in isolated patches⁴⁰.

Critically, our data reveals widespread metric discordance: 58% of grid cells exhibit conflicting impacts (e.g., stable cover but falling height) currently, rising to 89% if viewed from the temporal trend (Supplementary Fig. 11, Note 1). This directly demonstrates that area-based assessments miss non-area dimensions of forest degradation. Forest height is also critical for maintaining balanced biodiversity and ecological structure. While it is true that some specialists—such as understory frugivores or early-successional insects—may benefit from reduced canopy height and increased light penetration in young or disturbed forests, these gains may be localized³². More broadly,

reduced height disrupts fine-scale canopy-understory niche partitioning⁴¹: tall forests support unique assemblages (e.g., canopy-dwelling birds, epiphytes, and arboreal mammals) that depend on vertical stratification, while their loss cannot be offset by increases in early-successional species. This imbalance is compounded by linked declines in NPP, which impairs carbon sequestration^{31,42}, and reduces resource availability (e.g., floral nectar, leaf litter) that sustains both canopy and understory communities.

Stratifying height dynamics by forest state—explicitly focusing on cells that retained forest cover throughout the study period (stable) and separately analyzing fully deforested cells (lost) and newly established forest (gained)—reinforces this complexity. Relative to references, forests gained in road zones are shorter than lost ones (Supplementary Fig. 12), reflecting the replacement of tall mature trees

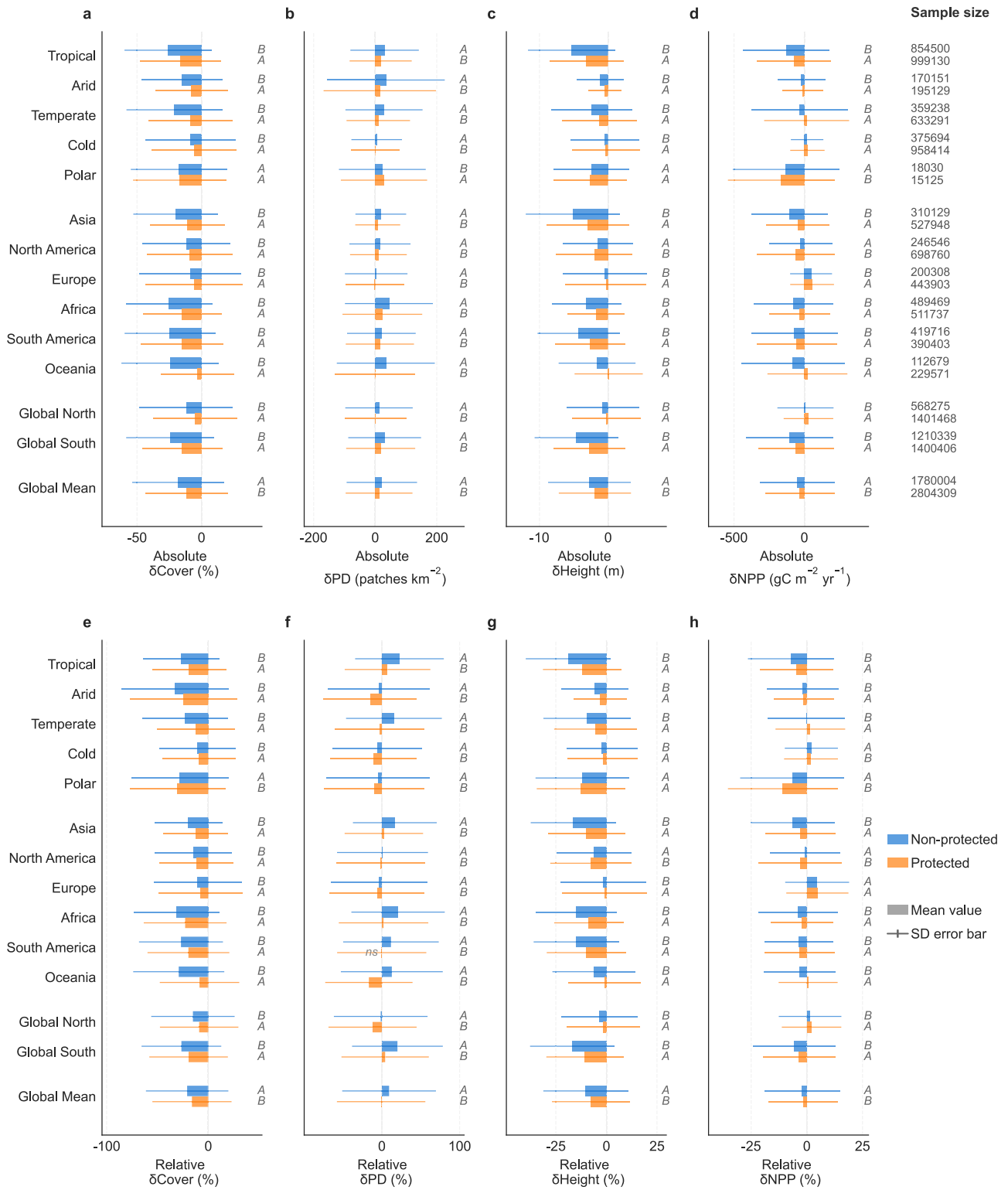


Fig. 6 | Contrasting road impacts on current forest structure and function between protected and non-protected reference areas. a–d Absolute changes and **e–h** normalized relative changes in forest metrics. References were defined as 5-km buffer zones surrounding protected areas. Data are presented as mean values \pm standard deviation (SD). Mean estimates for all groups differ significantly from zero (two-sided one-sample *t*-test, $P < 0.05$), except one marked ‘ns’.

Uppercase italic gray letters indicate significant differences between protected areas and non-protected references (one-way ANOVA followed by Tukey’s HSD test; distinct letters denote significant differences at $P < 0.05$). δ denotes differences between road areas and background references. Source data are provided as a Source Data file.

with young regrowth or plantations. More importantly, stable road-zone forests still show globally lower heights than reference areas. This provides evidence of “cover-neutral degradation”—such as selective logging of mature trees (removing tall individuals while retaining overall cover) or edge-related growth suppression^{15,43,44}—that area-only metrics overlook. This structural change also varies temporally and regionally: stable tropical road-zone forests show declining heights (consistent with ongoing selective extraction), particularly in South America and Africa, while temperate and boreal ones exhibit increases (linked to restoration or managed growth). This divergence aligns with broader discordance patterns, driven by unregulated extraction in the tropics versus restoration policies in temperate regions. It emphasizes that road impacts require context-specific, multidimensional assessment.

Socioeconomic governance shapes regional variability in road impacts

Road-linked forest impacts exhibit striking global variability, with socioeconomic governance mediating biophysical vulnerabilities. Biophysical baselines set inherent risk: tropical forests show the largest absolute cover and height declines due to high baselines (Supplementary Fig. 3), while arid zones have the steepest PD increases driven by naturally fragmented forest landscapes⁴⁵ (reflected in higher arid reference PD) (Supplementary Fig. 3). Yet governance—via policy, enforcement, and development priorities—ultimately shapes these impacts.

Governance drives road impacts through two linked pathways: direct construction disturbance, and indirect clearing or forestation enabled by improved access to remote forests. This access facilitates agriculture, logging, and urbanization^{3,8,9,18}, captured in the non-linear relationship between the Human Footprint Index (i.e., HFI) and degradation. Below an HFI of -0.4, rising pressure exacerbates degradation—consistent with unregulated logging in low-governance tropical regions^{13,21,46}. Above this threshold, impacts on height and NPP weaken (Fig. 5), reflecting a “development transition” toward protection and restoration⁴⁷, as exemplified by urban greenspace expansion⁴⁸.

This transition is most evident in the Global North, where structural improvement in low-HFI high-latitude regions stems from two governance-enabled drivers: (1) policy-led restoration of historically logged areas^{49,50}; and (2) reduced agricultural and fuelwood demand⁵¹. The latter reflects domestic shifts (e.g., reduced land-intensive farming, mechanization) and globalization of resource consumption—nations in the Global North source soy, palm oil, and timber from the Global South via international trade^{46,52,53}. This “offshoring” of agricultural land use reduces pressure on domestic forests, creating space for reforestation in the Global North while shifting road-driven deforestation to the Global South with weaker land-use regulations. By contrast, unplanned road expansion proceeds largely unconstrained in low-governance areas (e.g., tropical Africa, Southeast Asia), explaining their steepest declines in height and NPP. Regionally, improvements to forests in the Global North are further linked to intensive timber plantations (e.g., Scandinavian conifers), where managed growth (thinning, replanting) boosts structural metrics near roads⁵⁴, whereas Global South plantations—nearly four times more extensive (Supplementary Fig. 13)—show steeper declines in height and NPP (Supplementary Fig. 14) due to lower governance standards and/or the use of inherently shorter plantation species (e.g., oil palm, *Acacia mangium*) compared to the natural forests in these regions.

Beyond governance, two factors may modify the observed road impacts. First, reference bias may inflate perceived gains: this bias stems from complex terrain (causing edge density differences) and uneven distribution of reference pixels used to estimate road impacts (Supplementary Fig. 15). Alongside unaccounted microclimatic improvements (e.g., increased light/temperature at road edges), these

factors favor fast-growing pioneers in high latitudes, potentially overstating restoration success^{55,56}. Second, climate change interacts with governance to create a “dual buffer” in boreal regions: rising temperatures extend growing season length and alleviate thermal constraints on photosynthesis, boosting growth rates of conifers⁵⁷. For example, future projections for Canadian boreal forests suggest 20.5–22.7% warming-induced growth increases⁵⁸. The warming-induced growth enhancement partly offset the impacts of road disturbance. This interaction is unique to high latitudes, where boreal forests, having evolved under cold stress and natural disturbances (wildfires, permafrost thaw), are adapted to recover via accelerated growth after disturbance. In contrast, tropical forests operate near their thermal optima; further warming reduces photosynthetic efficiency and exacerbates drought stress^{14,59}, thereby amplifying road-driven degradation (e.g., Amazon edge mortality).

However, structural recovery in high-latitude regions masks critical non-structural ecological risks. Roads fragment movement corridors for large mammals—such as caribou and brown bears—that depend on contiguous boreal habitats⁶⁰, reducing population connectivity despite increased tree height, with long-term implications for genetic diversity and species viability. Disturbed road edges also facilitate invasion of non-native species (e.g., *Rhamnus cathartica*)⁶¹, which outcompete native vegetation, alter soil nutrient cycling, and disrupt trophic networks. These impacts, invisible to structural metrics like cover and height, erode ecological integrity—reinforcing the need for multidimensional assessments that integrate climate dynamics, vegetation structure, and faunal/community processes to fully capture the breadth of road-associated effects.

These findings suggest that road-linked degradation is a product of governance choices, not inevitability. Mitigation requires context-specific action: protecting intact forests in low-HFI regions to avoid crossing degradation thresholds; upgrading plantation standards in the Global South to move beyond “cover-first” policies; and scaling evidence-based restoration globally. Strengthening governance capacity in the Global South, alongside addressing offshored deforestation, will be critical to reconciling infrastructure development with forest conservation.

Tropical rainforests: Escalating threats from undercounted roads and the urgency of conservation action

Tropical rainforests are disproportionately vulnerable to road-linked degradation, despite not always showing the largest absolute metric changes. This vulnerability stems from their ecological importance, socioeconomic drivers, and ongoing infrastructure expansion. First, global biodiversity and carbon hotspots^{11,12}, even localized road disturbance has outsized impacts: tropics exhibit the highest per-unit degradation (Fig. 2) and contribute most to global road-linked loss (Supplementary Fig. 6). Second, tropical economies rely heavily on agricultural and forestry exports³¹. Demand fuels deforestation along roads, particularly in hotspots like the Brazilian Amazon^{13,16,19,23,40,53}. Critically, roads are often constructed explicitly to access timber and arable land^{4,15}, creating a feedback loop where infrastructure enables further exploitation. This contrasts with restoration-driven recovery in Europe and southern China^{13,16,20}. Third, tropics are the epicenter of recent road expansion^{4,10}, signaling worsening fragmentation and loss of ecosystem services.

Our tropical degradation estimates are likely conservative due to “ghost roads”—informal or illegal routes absent from official datasets. In tropical Asia-Pacific, actual road lengths are 3.0–6.6 times greater than recorded². Nearly 100% of roads in parts of Indo-Malaysia were previously unmapped²⁵. Even with improved OpenStreetMap data, “ghost roads” persist. This is evidenced by substantial forest loss ≥ 5 km from documented roads (Supplementary Fig. 16), a distance typically considered insulated from road impacts^{14,33}. Natural disturbances like wildfires and insects contribute minimally to this loss relative to road-

enabled human activity¹⁸, confirming that unaccounted infrastructure drives underestimation. These findings together highlight an urgent, underrecognized threat: escalating, undercounted road expansion in tropics risks irreversible losses to climate stability and biodiversity. Addressing this requires mapping informal roads, restricting unnecessary infrastructure in intact forests, and aligning development with conservation.

Beyond protected areas: The need for integrated transport-forest planning

Protected areas (i.e., PAs) are a cornerstone of global conservation⁶², and their value is clear in current forest conditions: globally, road-linked degradation (e.g., cover loss, fragmentation) is significantly milder within PAs than in adjacent non-protected areas. This protective effect—driven by regulatory safeguards and restricted access—confirms that PAs still mitigate road impacts more effectively than unprotected lands overall. Yet their ability to curb worsening degradation since 2000 varies drastically by region, revealing critical limitations in boundary-only protection. In temperate and cold biomes, PAs have successfully slowed escalating road-driven decline: their remote locations (reducing development pressure) and stricter enforcement of access restrictions have stabilized forest structure⁶³. By contrast, tropical PAs have largely failed to halt worsening degradation—South American PAs, for example, saw sharp increases in road-linked forest loss and fragmentation between 2000 and 2020^{2,9,64}. Tropical PAs failure stems from overlapping pressures: rising demand for timber and agricultural land, weak law enforcement, scarce forest outside PAs, and the allure of in-PA resources. These fuel illegal logging and encroachment⁶⁵. Even biodiversity-rich nations like Brazil—a signatory to multilateral environmental agreements since the 1990s—struggle to prevent deforestation^{6,66}. This highlights the need to move beyond boundary-based protection to integrated transport-forest planning.

Given inevitable future road expansion¹⁰ and current conservation gaps⁶⁶, we advocate strategic road planning to concentrate human activity and mitigate roadless area disturbance⁶⁷. Our data support this: 2000–2020 increases in NTL and HFI, as well as the forest loss and gain, are concentrated in road zones, especially in South America and Asia (Supplementary Fig. 17). Effective planning balances stakeholder interests by prioritizing roads in degraded, agriculture-dominated landscapes. This improves market access, reduces waste, and diverts migration from pristine forest fringes⁶⁸ while avoiding intact forests. By integrating current forest condition and road exposure risk (Supplementary Fig. 18 and Note 2), we identify clear priorities: conserve tropical forests in the Brazilian Amazon, Central Africa, and South Asia (Supplementary Fig. 19); restore high-exposure, poor-condition regions like parts of Europe, India, and eastern China. This approach reconciles development needs with forest protection.

Addressing gaps in road-forest impact assessments

This study advances understanding of global road-linked forest degradation, but key uncertainties and data gaps require future work. First, data limitations prevented distinguishing natural forest conversion to plantations. Despite their expansion from 4% to 7% of global forest area (1990–2020)⁶⁹, current products do not differentiate primary, regenerating, and plantation forests. This likely underestimates degradation¹⁷. Second, unaccounted disturbances—wildfires, insects, and human activity—in road and roadless areas introduce bias. Wildfires drive high-latitude loss²², and while grid cells with >10% cover loss were excluded from references (Methods), regenerating forests may skew baselines. Road impacts extending ≥ 5 km³³ and disproportionate “Other” region loss (Supplementary Fig. 16b) further suggest underestimation. Third, lack of reference areas excluded a large fraction of forests in Europe, eastern U.S., eastern China, and India (Supplementary Fig. 2c, e). These regions have high human activity, so degradation

is likely substantial. Finally, absent time-series transportation datasets hinder lifecycle assessments (construction, operation, decommissioning), conflating distinct impact phases. Addressing these gaps will require integrating advanced remote sensing—such as hyperspectral mapping for forest type differentiation and development of high-resolution disturbance maps—with improved transportation datasets. Refining the GEM-BR method to account for confounding disturbances will also help. This work will enhance assessment accuracy and support evidence-based conservation.

Concluding remarks

This study provides a global quantification of transportation infrastructure impacts on forest structure and function, revealing road-linked multidimensional degradation—reduced canopy cover, tree height, and NPP, plus increased fragmentation—shaped by biophysical vulnerability and socioeconomic governance. Tropical regions bear the brunt: highest per-unit impact, 54.8% of global road-associated forest loss, and steepest degradation since the 2000s—driven by unregulated road expansion for agriculture/timber and weak protected area enforcement, with impacts likely underestimated by uncounted “ghost roads.” In contrast, the Global North shows muted effects and some signs of structural recovery, as legacy road networks limit new disturbance, international trade reduces domestic land use pressure, and restoration policies drive resilience. Metric discordance (e.g., “cover-neutral degradation”) reveals that area-based assessments alone miss road-associated changes. These results indicate that road-linked forest degradation is a governance choice, not an inevitability. We advocate integrated transport-forest planning: prioritize roads in degraded landscapes, protect tropical hotspots (Amazon, Central Africa, South Asia) via mapping/regulating informal roads, strengthen tropical PA enforcement, and restore high-exposure regions. Centering the multidimensional metrics and governance in infrastructure decisions is key to balancing development with safeguarding forests as carbon sinks and biodiversity strongholds—critical for global climate and conservation goals.

Methods

Datasets

The global transportation infrastructure is based on two primary geospatial datasets: OpenStreetMap (OSM)³⁴ and Version 4 of the Global Roads Inventory Project (GRIP4)¹⁰. Established in 2004, OSM is an open-access, crowd-sourced database of worldwide roads, regularly updated by a vast network of individual volunteers worldwide. Over the years, the accuracy of OSM has markedly improved, owing to contributions from organized corporations and humanitarian mapping communities⁷⁰. It is now regarded as the most reliable and comprehensive global road dataset^{71,72}, extensively utilized for various purposes such as urban planning, sustainable development, environmental monitoring, public health initiatives, web mapping, and navigation services. For this study, we obtained the OSM database in Shapefile format from the Geofabrik download server, with the latest update timestamped June 25, 2024. We included all automobile-suitable road types (e.g., primary roads, secondary roads, highway links, and residential/service roads) and all railway corridors. Non-automobile paths (e.g., bridleways, cycleways, footways) were excluded, as these features exhibit high spatial incompleteness in OSM and have minimal influence on forest clearance. GRIP4, by contrast, was developed through the harmonization and integration of nearly 60 geospatial road infrastructure datasets—sourced from publicly available national and supranational vector datasets provided by governments, research institutes, non-governmental organizations (NGOs), and crowdsourcing initiatives—with OSM among its core input sources¹⁰. This harmonization process standardized spatial attributes (e.g., road class, connectivity) across heterogeneous datasets, yielding a unified global road inventory.

Forest structure metrics—such as forest cover, patch density (PD), and height—were quantified using the 30-m GLAD Global Land Cover and Land Use Change datasets for the years 2000 and 2020^{73,74}. These datasets, encompassing forest extent, forest height, cropland, built-up areas, surface water, and perennial snow and ice extent, were derived from GLAD Landsat Analysis Ready Data employing machine learning techniques and validated against a statistical sample of reference data, achieving user's and producer's accuracies above 85%, except for built-up areas⁷³. Forests were defined to include wildland, managed, and planted tree cover, incorporating agroforestry and orchards. Forest extent maps were generated by assigning grid cells with a forest height of ≥ 5 meters as the “forest” land cover class, aligning with the Food and Agriculture Organization of the United Nations (FAO) definition.

We computed forest cover, PD, and height at a 1 km grid scale using ArcGIS 10.8.1 (Esri, Redlands, CA, USA) for spatial zonal statistics and indicator extraction: this choice was driven by both the need to calculate PD (which requires a spatial unit large enough to contain multiple contiguous forest patches, aligning with landscape ecology conventions where PD is typically quantified at scales ranging from 500 m to 10 km to balance patch detectability and ecological relevance^{75,76}) and to maintain compatibility with complementary datasets that are primarily available at kilometer-scale resolutions. For forest cover, we used the percentage of a 1 km grid cell occupied by forest (rather than binary classification) to retain sensitivity to subtle changes; PD was calculated by assigning unique identifiers to each contiguous forest patch and counting these identifiers per 1 km cell; and mean height was derived by averaging height values across all 30 m forest pixels within each 1 km grid cell.

The forest function indicator of NPP was derived from the Version 6.1 MODIS NPP dataset at a 500 m pixel resolution (MOD17A3HGF)⁷⁷. NPP, defined as the net carbon gain by plants, has been widely used to measure ecosystem function⁷⁸. Mean NPP values from 2001 to 2003 and from 2019 to 2021 were used to assess forest productivity at the beginning and end of the study period, respectively.

Environmental factors—encompassing soil, climate, and topographic properties—were used to screen the background reference for forests adjacent to roads (see detailed Methods in subsequent sections). Soil parameters were acquired from SoilGrids Version 2 at a spatial resolution of 250 m. SoilGrids is a global digital soil mapping system that employs state-of-the-art machine learning methods to map the spatial distribution of soil properties worldwide⁷⁹. The outputs of SoilGrids consist of global soil property maps across six standard depth intervals. We calculated mean soil parameters loosely by assigning weights reflective of vegetation root distributions (and thus relevance to vegetation growth)^{80,81}: 0.15 for 0–5 cm, 0.25 for 5–15 cm, 0.25 for 15–30 cm, 0.15 for 30–60 cm, 0.10 for 60–100 cm, and 0.10 for 100–200 cm. Climate variables were derived from CHELSA (Climatologies at High Resolution for the Earth's Land Surface Areas) Version 2.1 for the period 1981–2010⁸². CHELSA is a very high-resolution (~1 km) global downscaled climate dataset currently hosted by the Swiss Federal Institute for Forest, Snow and Landscape Research WSL, designed to provide free access to high-resolution climate data for research and applications, with continuous updates and refinements⁸². Topographic features were derived from Version 3 of the Advanced Spaceborne Thermal Emission and Reflection Radiometer (ASTER) Global Digital Elevation Model (GDEM), which has a native spatial resolution of 30-m⁸³. All environmental datasets were upscaled to a 1 km spatial resolution using ArcGIS 10.8.1 for resampling to ensure consistency with the spatial scale of forest metrics.

A global dataset of plantations—comprising tree crops and planted forests—with establishment years spanning 1982–2020⁸⁴ was additionally used for two purposes: (1) refining the selection of background reference forests, and (2) supporting analyses of potential differences in road impacts between natural forests and planted systems. This dataset was developed using the LandTrendr algorithm on

the Google Earth Engine (GEE) platform, with a native spatial resolution of 30 m.

To quantify human pressure linked to road-forest change, we used the ~1 km resolution machine learning-based HFI (ml-HFI) for 2000 and 2019²⁹—selected for its alignment with our global, dynamic analysis needs. Trained via CNNs on Hansen Global Forest Change (GFCv1.7) imagery²⁰, the ml-HFI (0–1, low-to-high pressure) avoids the original Williams-HFI's reliance on harmonizing eight multi-source sub-indices⁸⁵, simplifying data inputs drastically. It achieves high accuracy (mean absolute error = 0.07 on unseen data) with only 3% terrestrial training samples and enables near-real-time updates via GFCv1.7 compatibility—critical for capturing 2000–2019 human pressure dynamics tied to road expansion. We further used nighttime light (NTL) data—an effective proxy for human pressure, particularly socioeconomic activity and urbanization—to cross-validate findings based on ml-HFI. NTL datasets (30 arc-seconds spatial resolution) for 2000 and 2020 were obtained from a harmonized time series integrating Defense Meteorological Satellite Program (DMSP) and Visible Infrared Imaging Radiometer Suite (VIIRS) data³⁵.

The latest version of the World Database on Protected Areas (WDPA), last updated on September 20, 2023, was used to compare the effects of roads on protected versus non-protected regions⁸⁶. Renowned for its comprehensiveness, the WDPA serves as the premier global repository of marine and terrestrial protected area data, undergoing monthly updates. Data for the WDPA is sourced from international convention secretariats, governmental entities, and collaborative non-governmental organizations.

A recently published 1 km Köppen-Geiger climate zone map⁸⁷ was utilized to discern road impacts under various climatic conditions. The climate was classified into five main classes, including tropical, temperate, arid, cold, and polar. The Köppen-Geiger climate zone map has been widely used to delineate climate zones for global-scale studies.

Estimating road impacts on forest structure and function

A systematic framework was developed to quantify road impacts on forest structure and function, implemented in three sequential steps (Supplementary Fig. 1). First, the study domain was restricted to “forested” grid cells, defined as 1 km grid cells with forest cover > 0 in either 2000 or 2020. Regions with no forest cover during the study period (2000–2020) were excluded, even though some of these areas (e.g., eastern United States, Europe, and eastern China) may have experienced extensive historical forest loss. The spatial distribution of the selected forested grid cells is presented in Supplementary Fig. 2a. Forests present in 2020 are primarily distributed across tropical and cold biomes, accounting for nearly 80% of the total forested area (Supplementary Fig. 2b). At the continental scale, Asia and South America collectively contain more than half of the total 2020 forest extent, with a notable concentration in Global South nations.

Second, the land surface was broadly categorized into three distinct zones based on proximity to transportation infrastructure: road, road-reference interface (RRI), and “other” regions (Supplementary Fig. 2c). Drawing on established methods^{4,33}, the road zone was delineated as the immediate buffer within 1 km of roads—an area where forest ecosystems are likely to experience substantial impacts from road construction and/or operation. Given the documented incompleteness of current global transportation datasets^{2,70,71}, we supplemented OSM-derived road buffers with GRIP4 data. Incorporating GRIP4 increased the estimated road area by 11%, representing roads captured exclusively by GRIP4 (Supplementary Fig. 20). The RRI was defined as the 1–5 km buffer extending outward from the road zone—a distance range where forests have been shown to experience partial or minimal impacts from transportation infrastructure^{4,6,25,33}. To characterize how road impacts diminish with increasing distance from roads, the RRI was further subdivided into contiguous 1 km buffers (i.e., 1–2 km, 2–3 km, 3–4 km, and 4–5 km from roads). Forested areas

located > 5 km from roads were classified as “other”. These regions are presumed to experience no or minimal road-related impacts due to limited accessibility, making them suitable as potential reference areas. This designation is supported, in part, by comparable mean forest cover values between the “other” zone and the outer RRI zone (5 km buffer; Supplementary Fig. 2d). Approximately two-thirds of global forest extent falls within the road or RRI zones (Supplementary Fig. 2d). This pattern is particularly pronounced in Europe and North America, where ~50–60% of forests are located within the road zone.

Third, we quantified the road impact (δI) on forest structure and function using two complementary metrics—absolute disparities and normalized relative disparities—between forest metrics in road-influenced zones and their corresponding background reference values, calculated at the 1 km grid scale:

$$\text{Absolute } \delta I = I_{\text{road}} - I_{\text{ref}} \quad (1)$$

$$\text{Relative } \delta I = (I_{\text{road}} - I_{\text{ref}}) / (|I_{\text{road}}| + |I_{\text{ref}}|) * 100\% \quad (2)$$

where I denotes a given forest metric (i.e., cover, PD, height, or NPP), I_{road} is the value of the metric for a “forested” grid cell located in either the road zone or RRI area, and I_{ref} is the background reference value for that target cell. While I_{road} was directly extracted from the forest metrics datasets, no established method exists to estimate the I_{ref} . To address this gap, we developed the Grid-wise Environmental Matching for Background Reference (GEM-BR) method, a moving-window approach tailored to derive I_{ref} for each target forested cell in road/RRI zones (Supplementary Fig. 1).

The GEM-BR method is anchored in the ecological principle that forests experiencing near-identical environmental conditions will exhibit similar growth, structure, and function^{88,89} when unperturbed by anthropogenic disturbances like road development. To operationalize this “environmental similarity” criterion, we first defined a Comprehensive Environmental Index (CEI) that integrates three key environmental domains: climate (including multiyear mean precipitation, near-surface air temperature, surface downwelling shortwave radiation, and vapor pressure deficit), soil (clay content, sand content, soil depth, soil organic carbon content, pH, and cation exchange capacity), and topography (elevation, aspect, and slope). All environmental variables were normalized to a range of 0–1 to eliminate scale-dependent biases, after which we applied principal component analysis (PCA) to the normalized dataset. We retained principal components (PCs) with a cumulative variance contribution $\geq 85\%$ —a threshold selected to capture the majority of environmental variability while reducing dimensionality—and calculated CEI for each forested cell as the weighted sum of these retained PCs, with weights equal to the variance contribution of each PC.

To implement GEM-BR, we first partitioned global forested regions into non-overlapping 100 km \times 100 km primary windows and expanded each window by a 50 km buffer zone (forming an “extended window”) to ensure access to a sufficient pool of potential reference cells outside road/RRI zones. For every forested cell in each extended window, we computed CEI using the PCA-based method described above. We then screened potential reference cells for each target forested cell in road/RRI zones using a sequential set of constraints: candidates were first limited to cells within 50 km of the target but outside road/RRI zones (denoted as candidate pool N_1); from this pool, we retained the top 20% of cells with the smallest CEI difference from the target if $N_1 \geq 15$, or the top 3 cells with the smallest CEI difference if $N_1 < 15$ (ensuring robust similarity even in data-sparse regions). We further excluded candidates with absolute forest cover change (2000–2020) $\geq 10\%$ (to remove cells with severe deforestation or afforestation), fraction of plantation area (2000–2020) $\geq 10\%$ (to exclude intensively managed plantations), or detectable nighttime

lights (to exclude cells affected by unmeasured anthropogenic activity), and only retained target cells with ≥ 3 qualified candidates remaining after these filters (ensuring I_{ref} is derived from a statistically meaningful sample).

For target cells meeting all criteria, I_{ref} was computed as the inverse distance-weighted (IDW) means of the reference values—assigning higher weights to cells closer to the target to ensure robust background matching. Approximately 40% of forested cells in road/RRI zones were excluded from subsequent impact analyses due to insufficient reference cells (failing the ≥ 3 candidates filter), as detailed in Supplementary Fig. 2e.

In addition, we assessed the sensitivity of estimated road impacts on forests by defining an expanded RRI zone of 1–10 km (hereafter referred to as RRI₁₀). Results indicate that the estimated road impacts on forest metrics (Supplementary Fig. 2f) are highly consistent in terms of direction, magnitude, and spatial pattern of changes in current forest state when comparing RRI₁₀ with the original 1–5 km RRI definition (hereafter RRI₅; Supplementary Fig. 2f–i). Nonetheless, the remaining forest area in the road zone under RRI₁₀ is only 45% of that under RRI₅ (Supplementary Fig. 2f), indicating that most forested cells in the road zone would be excluded if adopting the RRI₁₀ definition. Furthermore, using RRI₁₀ introduces substantial bias in the magnitudes of long-term temporal changes—particularly for δ PD and δ Height (Supplementary Fig. 2f–t). We therefore prioritize RRI₅ for this study for two reasons: (1) it retains a far larger number of forested grid cells for the final analysis, ensuring robust statistical power; and (2) in most cases, road impacts exhibit a clear stable trend when buffer distances extend beyond 5 km, justifying the 5 km upper bound for the RRI zone (Supplementary Fig. 2f). Notably, all statistical computations were implemented in Python 3.12 with core libraries (pandas, numpy, scipy, sklearn).

Analysis

To evaluate road impacts on forest ecosystems, we analyzed two dimensions of four key road impact metrics— δ Cover, δ PD, δ Height, and δ NPP (where δ denotes the difference between road-influenced zones and matched background reference areas identified via the GEM-BR strategy): current state (2020) and long-term temporal changes (2000–2020). Road-influenced zones were defined as 1 km buffers adjacent to roads, consistent with the core study extent; we further assessed distance decay effects up to 5 km to quantify the total impact area.

The current state of road impacts was quantified using 2020-specific impact estimates for each metric. For long-term temporal changes, we first derived the absolute values of these four metrics for both 2000 and 2020, and then used these two time points as baselines to compute two types of change indicators: absolute temporal change ($\Delta\delta I = \delta I_{2020} - \delta I_{2000}$), which reflects the raw magnitude of shifts in road impact intensity, and normalized relative temporal change ($(\delta I_{2020} - \delta I_{2000}) / (|\delta I_{2020}| + |\delta I_{2000}|) * 100\%$), which standardizes change magnitudes to a [–100, 100]% range to enable cross-metric comparison.

For δ Cover specifically, we extended the analysis to include the net gain and net loss of forest within road-influenced zones over 2000–2020, to disentangle whether road impacts manifest more strongly in forest loss or suppressed gain. For δ Height, we further stratified the analysis by forest change type: we compared height disparities (relative to background reference forests) across three forest subsets—stable forests (retaining cover throughout 2000–2020), gained forests (newly established post-2000), and lost forests (converted to non-forest by 2020)—to isolate road impacts on retained vegetation (distinct from newly regenerated or deforested areas) as highlighted in our analysis of structural degradation.

Spatial variations in road impacts were examined across five nested organizational scales: latitudinal gradients, continents, climate

zones (sensu Köppen-Geiger classification), Global North (i.e., developed) vs. Global South (i.e., developing) regions, and individual countries. The division between Global North and Global South is based on socioeconomic and political characteristics, following the classification framework of the United Nations Conference on Trade and Development (UNCTAD). For statistical validation of these spatial patterns, we employed two complementary tests: (1) one-sample t tests to assess whether the mean road impact (δI) for each forest metric in each region differed statistically significantly from zero; (2) one-way analysis of variance (ANOVA) to evaluate whether there were significant differences in mean δI values across subregions within each scale. All statistical tests were conducted at a significance level of $\alpha = 0.05$, with post-hoc Tukey's HSD tests to pinpoint pairwise differences between subregions.

We further investigated the relationship between road impacts and human activity intensity, where human activity was quantified using two metrics: the 2019 HFI and 2020 NTL data (Supplementary Fig. 22). For this analysis, HFI values were binned into 100 intervals with an approximate width of 0.01, and NTL values into 63 intervals with a width of 1, to standardize the range of human activity intensity for correlation testing. In addition, we compared road impacts between protected and non-protected forest areas. To establish a comparable reference for non-protected forests, we defined forested cells within 5 km buffer zones around protected areas as “non-protected reference cells” (Supplementary Fig. 23). Protected areas smaller than 5 km² were excluded from this comparison to ensure an adequate sample size for robust statistical analysis. All statistical tests (e.g., t tests, ANOVA, correlation analyses) and result aggregation were conducted in Python 3.12, with visualization supported by matplotlib and seaborn.

Reporting summary

Further information on research design is available in the Nature Portfolio Reporting Summary linked to this article.

Data availability

All the processed source data generated in this study (supporting bar, column, line charts, and statistical analyses) are available as a Source Data file. The raw public datasets used in this study are available in their respective official or recommended public repositories under the following persistent access links/DOIs: OpenStreetMap (OSM) vector road data in Geofabrik (<https://download.geofabrik.de/>); Global Roads Inventory Project 4 (GRIP4) dataset in the GLOBIO information portal (<https://www.globio.info/download-grip-dataset/>); GLAD Global Land Cover and Land Use Change (GLCLUC2020) datasets in the University of Maryland's GLAD Laboratory (<https://glad.umd.edu/dataset/GLCLUC2020/>); MOD17A3HGF V061 product in NASA's EOSDIS Land Processes Distributed Active Archive Center (LP DAAC) (<https://lpdaac.usgs.gov/products/mod17a3hgfV061/>)⁷⁷; SoilGrids Version 2 in the International Soil Reference and Information Center (ISRIC) (<https://files.isric.org/soilgrids/latest/>); CHELSA Version 2.1 in the CHELSA Climate Portal (<https://www.chelsa-climate.org/>)⁹⁰; ASTER Global Digital Elevation Model (GDEM) Version 3 in NASA Earthdata Search (<https://search.earthdata.nasa.gov/>); 2019 Human Footprint Index (ml-HFI) data in the Mountain Scholar repository (<https://hdl.handle.net/10217/216207>)⁹¹; 2020 nighttime light datasets in Figshare (<https://doi.org/10.6084/m9.figshare.9828827.v2>)⁹²; World Database on Protected Areas (WDPA) in Protected Planet (<https://www.protectedplanet.net/en/>); Köppen-Geiger climate zone map in the GLOH2O portal (<https://www.gloh2o.org/koppen/>); and Version 2 global map of plantation establishment years (1982–2020) in Figshare (<https://doi.org/10.6084/m9.figshare.19070084.v2>)⁹³. Large spatial distribution raster datasets are not provided in the Supplementary Information or Source Data file due to their substantial file sizes, but are openly accessible via the original public repositories listed above. All DOIs for datasets have been included in the Reference list. No

access restrictions apply to any of the minimum dataset necessary for interpreting, verifying, or extending the research—all data are freely available without undue qualifications. Source data are provided in this paper.

Code availability

The Python code used to calculate the Comprehensive Environmental Index (CEI) and quantify road impacts in road/RRI zones, along with example data to support reproducibility of the analyses in this study, is publicly available via GitHub (<https://github.com/DechengZHOU/RoadImpactsForests.git>). The exact version (v1.0.0) used in the manuscript has been assigned a permanent, citable DOI and is included in the reference list⁹⁴. The code is provided for non-commercial, academic research purposes only, with permission for use, modification, and redistribution provided appropriate attribution to the original authors and this study is included. Unauthorized re-publication or commercial exploitation of the code is prohibited.

References

- Thacker, S. et al. Infrastructure for sustainable development. *Nat. Sustain.* **2**, 324–331 (2019).
- Engert, J. E. et al. Ghost roads and the destruction of Asia-Pacific tropical forests. *Nature* **629**, 370–375 (2024).
- Forman, R. T. T. & Alexander, L. E. Roads and their major ecological effects. *Annu. Rev. Ecol. Syst.* **29**, 207–231 (1998).
- Kleinschroth, F., Laporte, N., Laurance, W. F., Goetz, S. J. & Ghazoul, J. Road expansion and persistence in forests of the Congo Basin. *Nat. Sustain.* **2**, 628–634 (2019).
- Laurance, W. F., Goosem, M. & Laurance, S. G. W. Impacts of roads and linear clearings on tropical forests. *Trends Ecol. Evol.* **24**, 659–669 (2009).
- Tisler, T. R., Teixeira, F. Z. & Nóbrega, R. A. A. Conservation opportunities and challenges in Brazil's roadless and railroad-less areas. *Sci. Adv.* **8**, eabi5548 (2022).
- Vilela, T. et al. A better Amazon road network for people and the environment. *Proc. Natl. Acad. Sci. USA* **117**, 7095–7102 (2020).
- Laurance, W. F. et al. A global strategy for road building. *Nature* **513**, 229–232 (2014).
- Li, W. et al. Human fingerprint on structural density of forests globally. *Nat. Sustain.* **6**, 368–379 (2023).
- Meijer, J. R., Huijbregts, M. A., Schotten, K. C. & Schipper, A. M. Global patterns of current and future road infrastructure. *Environ. Res. Lett.* **13**, 064006 (2018).
- Myers, N., Mittermeier, R. A., Mittermeier, C. G., da Fonseca, G. A. B. & Kent, J. Biodiversity hotspots for conservation priorities. *Nature* **403**, 853–858 (2000).
- Pan, Y. et al. The enduring world forest carbon sink. *Nature* **631**, 563–569 (2024).
- Ma, J., Li, J., Wu, W. & Liu, J. Global forest fragmentation change from 2000 to 2020. *Nat. Commun.* **14**, 3752 (2023).
- Bourgoin, C. et al. Human degradation of tropical moist forests is greater than previously estimated. *Nature* **631**, 570–576 (2024).
- Lapola, D. M. et al. The drivers and impacts of Amazon forest degradation. *Science* **379**, eabp8622 (2023).
- Vancutsem, C. et al. Long-term (1990–2019) monitoring of forest cover changes in the humid tropics. *Sci. Adv.* **7**, eabe1603 (2021).
- Betts, M. G. et al. Quantifying forest degradation requires a long-term, landscape-scale approach. *Nat. Ecol. Evol.* **8**, 1054–1057 (2024).
- Curtis, P. G., Slay, C. M., Harris, N. L., Tyukavina, A. & Hansen, M. C. Classifying drivers of global forest loss. *Science* **361**, 1108–1111 (2018).
- Fischer, R. et al. Accelerated forest fragmentation leads to critical increase in tropical forest edge area. *Sci. Adv.* **7**, eabg7012 (2021).

20. Hansen, M. C. et al. High-resolution global maps of 21st-century forest cover change. *Science* **342**, 850–853 (2013).
21. Lewis, S. L., Edwards, D. P. & Galbraith, D. Increasing human dominance of tropical forests. *Science* **349**, 827–832 (2015).
22. McDowell, N. G. et al. Pervasive shifts in forest dynamics in a changing world. *Science* **368**, eaaz9463 (2020).
23. Pendrill, F. et al. Disentangling the numbers behind agriculture-driven tropical deforestation. *Science* **377**, eabm9267 (2022).
24. Potapov, P. et al. The last frontiers of wilderness: Tracking loss of intact forest landscapes from 2000 to 2013. *Sci. Adv.* **3**, e1600821 (2017).
25. Hughes, A. C. Have Indo-Malaysian forests reached the end of the road? *Biol. Conserv.* **223**, 129–137 (2018).
26. Broadbent, E. N. et al. Forest fragmentation and edge effects from deforestation and selective logging in the Brazilian Amazon. *Biol. Conserv.* **141**, 1745–1757 (2008).
27. Dantas de Paula, M., Groeneveld, J. & Huth, A. The extent of edge effects in fragmented landscapes: Insights from satellite measurements of tree cover. *Ecol. Indic.* **69**, 196–204 (2016).
28. Pan, Y., Birdsey, R. A., Phillips, O. L. & Jackson, R. B. The structure, distribution, and biomass of the world's forests. *Annu. Rev. Ecol. Evol. Syst.* **44**, 593–622 (2013).
29. Keys, P. W., Barnes, E. A. & Carter, N. H. A machine-learning approach to human footprint index estimation with applications to sustainable development. *Environ. Res. Lett.* **16**, 044061 (2021).
30. Brockerhoff, E. G. et al. Forest biodiversity, ecosystem functioning and the provision of ecosystem services. *Biodivers. Conserv.* **26**, 3005–3035 (2017).
31. Brinck, K. et al. High resolution analysis of tropical forest fragmentation and its impact on the global carbon cycle. *Nat. Commun.* **8**, 14855 (2017).
32. Martins, A. C., Willig, M. R., Presley, S. J. & Marinho-Filho, J. Effects of forest height and vertical complexity on abundance and biodiversity of bats in Amazonia. *For. Ecol. Manag.* **391**, 427–435 (2017).
33. Ibsch, P. L. et al. A global map of roadless areas and their conservation status. *Science* **354**, 1423–1427 (2016).
34. Haklay, M. & Weber, P. Openstreetmap: User-generated street maps. *IEEE Pervasive Comput.* **7**, 12–18 (2008).
35. Li, X., Zhou, Y., Zhao, M. & Zhao, X. A harmonized global nighttime light dataset 1992–2018. *Sci. Data* **7**, 168 (2020).
36. Hanski, I., Zurita, G. A., Bellocq, M. I. & Rybicki, J. Species–fragmented area relationship. *Proc. Natl. Acad. Sci. USA* **110**, 12715–12720 (2013).
37. Munguia-Rosas, M. A. & Montiel, S. Patch size and isolation predict plant species density in a naturally fragmented forest. *PLOS ONE* **9**, e111742 (2014).
38. Cote, J. et al. Evolution of dispersal strategies and dispersal syndromes in fragmented landscapes. *Ecography* **40**, 56–73 (2017).
39. Fahrig, L. et al. Is habitat fragmentation bad for biodiversity? *Biol. Conserv.* **230**, 179–186 (2019).
40. Haddad, N. M. et al. Habitat fragmentation and its lasting impact on Earth's ecosystems. *Sci. Adv.* **1**, e1500052 (2015).
41. Betts, M. G. et al. Global forest loss disproportionately erodes biodiversity in intact landscapes. *Nature* **547**, 441–444 (2017).
42. Crockett, E. T. H. et al. Structural and species diversity explain aboveground carbon storage in forests across the United States: Evidence from GEDI and forest inventory data. *Remote Sens. Environ.* **295**, 113703 (2023).
43. Matricardi, E. A. T. et al. Long-term forest degradation surpasses deforestation in the Brazilian Amazon. *Science* **369**, 1378–1382 (2020).
44. Assis, T. O. et al. CO₂ emissions from forest degradation in Brazilian Amazon. *Environ. Res. Lett.* **15**, 104035 (2020).
45. Aizen, M. A. & Feinsinger, P. Forest fragmentation, pollination, and plant reproduction in a Chaco dry forest, Argentina. *Ecology* **75**, 330–351 (1994).
46. Grantham, H. S. et al. Anthropogenic modification of forests means only 40% of remaining forests have high ecosystem integrity. *Nat. Commun.* **11**, 5978 (2020).
47. Crouzeilles, R. et al. A global meta-analysis on the ecological drivers of forest restoration success. *Nat. Commun.* **7**, 11666 (2016).
48. Wu, S., Chen, B., Webster, C., Xu, B. & Gong, P. Improved human greenspace exposure equality during 21st century urbanization. *Nat. Commun.* **14**, 6460 (2023).
49. Kaczan, D. J. Can roads contribute to forest transitions? *World Dev.* **129**, 104898 (2020).
50. Zhang, D. China's forest expansion in the last three plus decades: Why and how? *For. Policy Econ.* **98**, 75–81 (2019).
51. Pendrill, F. et al. Agricultural and forestry trade drives large share of tropical deforestation emissions. *Global Environ. Change* **56**, 1–10 (2019).
52. Kastner, T., Erb, K.-H. & Haberl, H. Rapid growth in agricultural trade: effects on global area efficiency and the role of management. *Environ. Res. Lett.* **9**, 034015 (2014).
53. Laso Bayas, J. C. et al. Drivers of tropical forest loss between 2008 and 2019. *Sci. Data* **9**, 146 (2022).
54. Kuliešis, A. et al. The impact of strip roads on the productivity of spruce plantations. *Forests* **9**, 640 (2018).
55. Meeussen, C. et al. Microclimatic edge-to-interior gradients of European deciduous forests. *Agric. For. Meteorol.* **311**, 108699 (2021).
56. Zhao, S., Liu, S. & Zhou, D. Prevalent vegetation growth enhancement in urban environment. *Proc. Natl. Acad. Sci. USA* **113**, 6313–6318 (2016).
57. Dial, R. J., Maher, C. T., Hewitt, R. E. & Sullivan, P. F. Sufficient conditions for rapid range expansion of a boreal conifer. *Nature* **608**, 546–551 (2022).
58. Wang, J., Taylor, A. R. & D'Orangeville, L. Warming-induced tree growth may help offset increasing disturbance across the Canadian boreal forest. *Proc. Natl. Acad. Sci. USA* **120**, e2212780120 (2023).
59. Bonan, G. B. et al. Reimagining earth in the earth system. *J. Adv. Model. Earth Syst.* **16**, e2023MS004017 (2024).
60. Fahrig, L. & Rytwinski, T. Effects of roads on animal abundance: An empirical review and synthesis. *Ecol. Soc.* **14**, 21 (2009).
61. Quiles, P. & Barrientos, R. Interspecific interactions disrupted by roads. *Biol. Rev.* **99**, 1121–1139 (2024).
62. Naughton-Treves, L., Holland, M. B. & Brandon, K. The role of protected areas in conserving biodiversity and sustaining local livelihoods. *Annu. Rev. Environ. Resour.* **30**, 219–252 (2005).
63. Andam, K. S., Ferraro, P. J., Pfaff, A., Sanchez-Azofeifa, G. A. & Robalino, J. A. Measuring the effectiveness of protected area networks in reducing deforestation. *Proc. Natl. Acad. Sci. USA* **105**, 16089–16094 (2008).
64. Meng, Z. et al. Post-2020 biodiversity framework challenged by cropland expansion in protected areas. *Nat. Sustain.* **6**, 758–768 (2023).
65. Asner, G. P., Lactayo, W., Tupayachi, R. & Luna, E. R. Elevated rates of gold mining in the Amazon revealed through high-resolution monitoring. *Proc. Natl. Acad. Sci. USA* **110**, 18454–18459 (2013).
66. Senior, R. A. et al. Global shortfalls in documented actions to conserve biodiversity. *Nature* **630**, 387–391 (2024).
67. Han, D., Attipoe, S. G., Han, D. & Cao, J. Does transportation infrastructure construction promote population agglomeration? Evidence from 1838 Chinese county-level administrative units. *Cities* **140**, 104409 (2023).
68. Laurance, W. F. & Balmford, A. A global map for road building. *Nature* **495**, 308–309 (2013).

69. FAO & UNEP. *The state of the world's forests 2020: Forests, biodiversity and people* (Food and Agriculture Organization of the United Nations, Rome, 2020).
70. Herfort, B., Lautenbach, S., Porto de Albuquerque, J., Anderson, J. & Zipf, A. A spatio-temporal analysis investigating completeness and inequalities of global urban building data in OpenStreetMap. *Nat. Commun.* **14**, 3985 (2023).
71. Barrington-Leigh, C. & Millard-Ball, A. The world's user-generated road map is more than 80% complete. *PLOS ONE* **12**, e0180698 (2017).
72. Hoffmann, M. T., Ostapowicz, K., Bartoń, K., Ibisch, P. L. & Selva, N. Mapping roadless areas in regions with contrasting human footprint. *Sci. Rep.* **14**, 4722 (2024).
73. Potapov, P. et al. The global 2000–2020 land cover and land use change dataset derived from the Landsat archive: First results. *Front. Remote Sens.* **3**, 856903 (2022).
74. Potapov, P. et al. Mapping global forest canopy height through integration of GEDI and Landsat data. *Remote Sens. Environ.* **253**, 112165 (2021).
75. Turner, M. G. & Gardner, R. H. (eds.) *Landscape ecology in theory and practice: Pattern and process* (Springer New York, New York, 2015).
76. Šimová, P. & Gdulová, K. Landscape indices behavior: A review of scale effects. *Appl. Geogr.* **34**, 385–394 (2012).
77. Running, S. W. & Zhao, M. MODIS/Terra net primary production gap-filled yearly L4 global 500m SIN grid V061 [Dataset]. NASA EOSDIS Land Processes Distributed Active Archive Center, <https://doi.org/10.5067/MODIS/MOD17A3HGF.061> (2021).
78. Hu, Z. et al. Shifts in the dynamics of productivity signal ecosystem state transitions at the biome-scale. *Ecol. Lett.* **21**, 1457–1466 (2018).
79. Poggio, L. et al. SoilGrids 2.0: producing soil information for the globe with quantified spatial uncertainty. *SOIL* **7**, 217–240 (2021).
80. Jackson, R. B. et al. A global analysis of root distributions for terrestrial biomes. *Oecologia* **108**, 389–411 (1996).
81. Luo, Z. et al. Evaluating soil water dynamics and vegetation growth characteristics under different soil depths in semiarid loess areas. *Geoderma* **442**, 116791 (2024).
82. Karger, D. N. et al. Climatologies at high resolution for the earth's land surface areas. *Sci. Data* **4**, 170122 (2017).
83. NASA. NASA/METI/AIST/Japan Spacesystems, and U.S./Japan ASTER Science Team. *ASTER global digital elevation model V003* (NASA Land Processes Distributed Active Archive Center, Sioux Falls, 2019).
84. Du, Z. et al. A global map of planting years of plantations. *Sci. Data* **9**, 141 (2022).
85. Williams, B. A. et al. Change in terrestrial human footprint drives continued loss of intact ecosystems. *One Earth* **3**, 371–382 (2020).
86. IUCN, UNEP-WCMC. *The world database on protected areas* (WDPA) (eds. Cambridge, UJ-W; IUCN, Gland, 2020).
87. Beck, H. E. et al. High-resolution (1 km) Köppen-Geiger maps for 1901–2099 based on constrained CMIP6 projections. *Sci. Data* **10**, 724 (2023).
88. Mitchell, J. C. et al. Forest ecosystem properties emerge from interactions of structure and disturbance. *Front. Ecol. Environ.* **21**, 14–23 (2023).
89. Saaty, T. L. Decision making with the analytic hierarchy process. *Int. J. Services Sci.* **1**, 83–98 (2008).
90. Karger, D. N. CHELSA-daily climate data at high resolution [Dataset]. *EnviDat*, <https://doi.org/10.16904/enviDat.687> (2025).
91. Keys, P. W., Barnes, E. A. & Carter, N. A machine-learning approach to human footprint index estimation with applications to sustainable development [Dataset]. Colorado State University Libraries, <https://doi.org/10.25675/10217/216207> (2021).
92. Li, X. C., Zhou, Y. Y., Zhao, M. & Zhao, X. Harmonization of DMSP and VIIRS nighttime light data from 1992–2018 at the global scale [Dataset]. *figshare*, 2020. <https://doi.org/10.6084/m9.figshare.9828827.v2>
93. Du, Z. R. et al. A global map of planting years of plantations [Dataset]. *figshare*, <https://doi.org/10.6084/m9.figshare.19070084.v2> (2022).
94. Zhou, D. et al. Code for global impacts of transportation infrastructure on forest degradation and loss (v1.0.0) [Computer software]. *Zenodo* <https://doi.org/10.5281/zenodo.17873268> (2025).

Acknowledgements

This work was supported by the National Natural Science Foundation of China (Grant No. 42571127; D.Z.), the National Key R&D Program of China (Grant No. 2021YFB2600100; L.H.), and the Hainan Talent Convergence Initiative (Grant No. HNYT20250005; S.L.). J.X. was supported by bridge support and the Iola Hubbard Climate Change Endowment from the University of New Hampshire.

Author contributions

D.Z., J.X., and S.Z. conceived the study and designed the research framework. D.Z. and L.Z. curated, processed, and analyzed the datasets. D.Z. drafted the initial manuscript. S.Z. supervised the entire research process. D.Z., J.X., S.L., L.H., J.F., and S.Z. contributed to data interpretation, manuscript drafting, and critical revision of intellectual content. All authors approved the final version for submission.

Competing interests

The authors declare no competing interests.

Additional information

Supplementary information The online version contains supplementary material available at <https://doi.org/10.1038/s41467-026-69150-4>.

Correspondence and requests for materials should be addressed to Jingfeng Xiao or Shuqing Zhao.

Peer review information *Nature Communications* thanks the anonymous reviewers for their contribution to the peer review of this work. A peer review file is available.

Reprints and permissions information is available at <http://www.nature.com/reprints>

Publisher's note Springer Nature remains neutral with regard to jurisdictional claims in published maps and institutional affiliations.

Open Access This article is licensed under a Creative Commons Attribution-NonCommercial-NoDerivatives 4.0 International License, which permits any non-commercial use, sharing, distribution and reproduction in any medium or format, as long as you give appropriate credit to the original author(s) and the source, provide a link to the Creative Commons licence, and indicate if you modified the licensed material. You do not have permission under this licence to share adapted material derived from this article or parts of it. The images or other third party material in this article are included in the article's Creative Commons licence, unless indicated otherwise in a credit line to the material. If material is not included in the article's Creative Commons licence and your intended use is not permitted by statutory regulation or exceeds the permitted use, you will need to obtain permission directly from the copyright holder. To view a copy of this licence, visit <http://creativecommons.org/licenses/by-nc-nd/4.0/>.

© The Author(s) 2026